TCAD device simulation of novel test structures for determining the lifetime in solar cells

Javid Aliyev, Ray Hueting, Rufat Alizada, Lis Nanver
Department of Semiconductor Components, University of Twente, Enschede, The Netherlands
(emails: j.aliyev@student.utwente.nl, r.j.e.hueting@utwente.nl)

***Abstract*—In this work a new device test structure for determining the charge carrier lifetime in solar cells is investigated using device simulations. This structure comprises a *pnp* phototransistor structure, which allows to determine the recombination or (effective) lifetime at the surface or in the shallow junction of the transistor. Several separate current components can be investigated, including that component solely determined by recombination at the surface, not possible in a standard diode or solar cell. Yet, the heart of this transistor basically imitates the solar cell. Investigating the current characteristics of the given structures and calculating the lifetime gives a clear explanation of the recombination process in solar cells, which is one of the main factors influencing the efficiency of solar cells.**

By examining the current density values calculated and simulated with different methods, the test structure is proven to be valid for the carrier lifetime investigation. A different outcome between a cylindrical and a 2D structure is observed, which can be attributed to base current spreading. The results indicate that a less uniform current flow is obtained for a wide cylindrical structure making this structure less suitable for lifetime extraction. The relation between current density and effective recombination along with the calculations of the sheet resistance are also presented.

This work is important for improving the solar cell efficiency.

***Index Terms*—Solar cell, carrier lifetime, surface recombination, phototransistor, base current, electron concentration, current density, TCAD.**

I. Introduction

THE worldwide demand for energy forces more and more people to rely on renewable energy sources rather than conventional ones. Solar cells appear to play a big role in satisfying today's growing energy demand in an environmentally benign way. But, for implementing those in a mass scale, further cost reduction is essential [1]. To reduce the costs many approaches have been considered, some of which affect the conversion efficiency of solar cells.

Surface recombination is one of the factors that influence efficiency of cells. Reducing the surface recombination leads to a longer carrier lifetime. The lifetime is a measure of how long a carrier is likely to stay around before recombining and is one of the most important parameters for the characterization of power electronic devices and photovoltaic solar cells. In particular, determining the lifetime plays an important role in optimization of solar cell performance. Therefore, a clear understanding of how many and where carriers are recombining is crucial for solar cell efficiency. However, determining the value and location of the (effective) lifetime in a solar cell, which is basically a diode, remains to be an issue. Surface recombination and lifetime in silicon devices have been studied and different lifetime extraction approaches were proposed [2], [3], [4]. However, the effect of carrier trapping on lifetime measurements should be taken into account. When traps are present, carriers tend to get trapped, but they do not recombine. Therefore, the measured apparent lifetime does not represent the actual recombination lifetime [5], and hence cause significant problems with the measurements [6].

In this work a dedicated *pnp* phototransistor structure, imitating a solar cell, is simulated in Silvaco's Technology Computer-Aided Design (TCAD) software [7]. The advantage of adopting device simulations is that the internal properties of the phototransistor can be investigated as a function of e.g. the geometrical parameters, doping concentration, locations and amount of traps. By varying these parameters one can see the effects of each aspect of the system. In addition, the existing test structures [9] can be optimized further by fine tuning several device parameters.

In this paper these test structures will be explained. The approach is to adopt the device simulation software to investigate the effect of lifetime or surface recombination on the device performance, thus, on efficiency of solar cells. The paper will conclude on whether this test structure is suitable for carrier lifetime investigation.

II. Test Structure

Figure 1 shows the schematic cross-section of the *pnp* phototransistor. We investigate both a 2D and a cylindrical structure with a constant radius $r = 68.5$ μm to the center of the active emitter layer, that is rotated around the indicated dashed line. The structure consists of two p^+-type emitters and a shallow p-type region, i.e. the active emitter region, in between. This region has been varied to investigate electron current density, using different methods elaborated in section III.

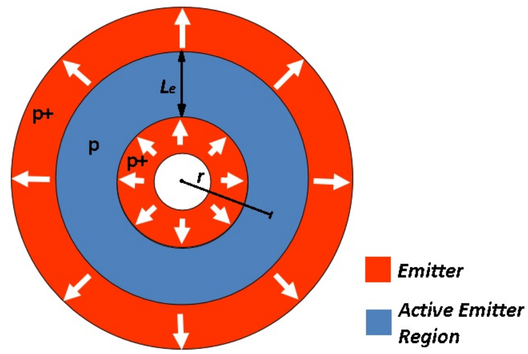

Fig. 2: The basic structure of the total p region.

TABLE I: Test parameters

Base contact width	2 μm
Emitter contact width	1 μm
Substrate thickness	200 μm
Base thickness	1 μm
n-type base doping	2e16 cm^{-3}
p-type substrate doping	1e15 cm^{-3}
Base doping implant	2.5e20 cm^{-3}
Emitter doping implant	1.5e20 cm^{-3}
Junction depth	0.0022μm
Temperature	300 K

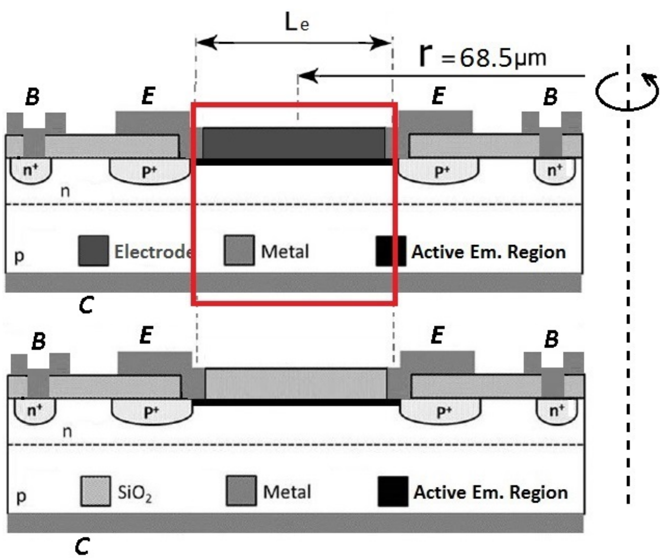

Fig. 1: Cross section of the test structures: (a) with electrode and (b) oxide layer. E and B indicate the emitter and base contact regions respectively.

Figure 1a illustrates a structure with an electrode on top of the active emitter region. By using an artificial electrode bulk and interfacial recombination effects are included in a single parameter called (effective) surface recombination velocity. Figure 1b shows a similar structure with an oxide layer instead of an artificial contact, which is more realistic and can be compared to real lifetime measurements. The purpose of using the first structure is to attract more electrons to the active emitter region and, hence, to better illustrate the electron current density extraction method explained in section III. The highlighted region in Figure 1a shows the part that imitates a diode, thus a solar cell. By analysing this structure, it is possible to investigate several separate current components and determine the carrier lifetime, which is not possible in real-life measurements of a standard diode or solar cell.

Figure 3 shows the zoomed-in device structure with the electrode with a surface recombination velocity of 10^2 cm/s constructed using Silvaco TCAD and plotted with Tonyplot. The length of the active emitter region, as well as many other parameters, such as device geometry, temperature, doping and surface recombination velocity (or lifetime), are included as variables. A variation of the electrode and oxide on top of the p layer has also been done. The doping profiles, like all other fixed parameters, are assumed to be uniform (see Table I).

The boron doping profile of the active emitter region was obtained from physical measurements. Its junction depth and peak doping concentration are shown in Table I. While simulating, 0.4 V (low injection) is applied to the emitter. Base and collector potentials are fixed to 0 V.

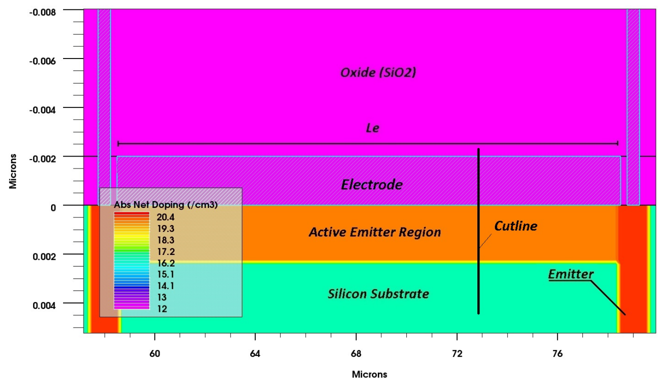

Fig. 3: Cross section of the test structure plotted with Tonyplot

III. Method

A. Electron current at interface

It is important to notice that the base current consists of two components: $I_\mathbf{n}$ and $I_\mathbf{p}$, where $I_\mathbf{n}$ is the electron current component from the base to emitter and $I_\mathbf{p}$ - the hole component from the emitter to base. Because of the special structure of the phototransistor, the electron base current itself also consists of two components: $I_\mathbf{n1}$ and $I_\mathbf{n2}$, where $I_\mathbf{n1}$ is the electron component from base to emitter and $I_\mathbf{n2}$ - to the active shallow emitter layer. Thus,

$$I_\mathbf{b} = I_\mathbf{p} + I_\mathbf{n} = I_\mathbf{p} + I_{\mathbf{n_1}} + I_{\mathbf{n_2}} \tag{1}$$

where $I_{\mathbf{n_2}} = J_{\mathbf{n_2}} \cdot A$, with A - area of the active emitter region.

In this work the second electron current component will be investigated, since this component is determined by the surface recombination. It is important to mention that surface recombination is a measure of the lifetime, as addressed in the appendix. To disentangle this component from the whole base current, the length of the active layer ($L_\mathbf{e}$) is varied (from 4 to 44μm). By varying this length, base current values corresponding to different $L_\mathbf{e}$ values can be determined. Further, it is shown that subtracting these $I_\mathbf{b}$ values leaves only $I_\mathbf{n2}$ component. From $\triangle I_\mathbf{b}$ vs $\triangle L_\mathbf{e}$ graph the electron current density can be calculated using:

$$J_\mathbf{n} = \frac{\triangle I_\mathbf{b}}{\triangle A} = \frac{\triangle I_\mathbf{b}}{2\pi r \cdot \triangle L_\mathbf{e}} \tag{2}$$

where r is the fixed radius of the emitter ring and $L_\mathbf{e}$ is the active emitter layer length.

To show that calculated $J_\mathbf{n}$ indeed corresponds to the second component of the electron current density, $J_\mathbf{n2}$ is extracted using the cutline function of Tonyplot (see Figure 3). A vertical line crossing the active emitter layer is used to look inside of the device, allowing direct determination of $J_\mathbf{n2}$.

Another method of obtaining this value is from 1D electron distribution inside the layer using the following formula [8]:

$$J_\mathbf{n2} = qD_\mathbf{n} \cdot \frac{(n_2 - n_1)}{d} \approx qD_\mathbf{n} \cdot \frac{n_2}{d} \tag{3}$$

where,

$$D_n = \frac{\mu_n k_\mathbf{B} T}{q} \tag{4}$$

with μ_n - mobility of electrons, k_B - Boltzmann's constant, T - temperature, D_n - diffusion constant and q - the elementary charge, d - diffusion length. The excess minority concentration n_2 at the base side of the active emitter layer has its maximum. Diffusion takes place resulting in an excess concentration smaller than n_2 [8]. The Silvaco software makes it possible to examine the distribution.

Same results obtained from different methods indicate that studying the active layer and investigating electron current component determined by the surface recombination is possible using the test device.

Alternatively, from electrons diffusing through a p-type region with an electrode [13], [14] or some non-ideal interface on top (see Figure 6), the relation between the electron current density and effective recombination velocity can be derived (see Appendix):

$$J_\mathbf{n} = \ q \cdot S_\mathbf{eff}(n_1 - n_0) \approx q \cdot S_\mathbf{eff} \cdot n_1, \tag{5}$$

where q is electron charge, $S_\mathbf{eff}$ is the effective recombination velocity, n_0 is the equilibrium concentration and n_1 is the concentration at the surface of the artificial contact or interface.

B. Sheet Resistance

The cylindrical test structures are also used to extract the sheet resistance of the active emitter region. In order to compare the simulation results with the measurement results from the lab, the electrode on top of the active emitter layer is replaced by an oxide layer with surface recombination velocity of 10^2 cm/s. To find the resistance, 0.4 V is applied to one of the emitter contacts and current through the active emitter region is simulated. From the slope of the resulting linear I-V curve the resistance can be determined. In transistors and other electronic devices, the contacts are part of the device, and contribute to the contact resistance. So, the simulated resistance consists of two components:

$$R_{\mathbf{m}} = R_{\mathbf{s}} + 2R_{\mathbf{c}}, \tag{6}$$

where $R_{\mathbf{s}}$ is the semiconductor resistance and $R_{\mathbf{c}}$ is the contact resistance.

The cylindrical ring structure has a fixed perimeter, therefore only two variables are important for the sheet resistance extraction: the measured resistance $R_{\mathbf{m}}$ of each structure and the active emitter region length $L_{\mathbf{e}}$. The contact resistance can be eliminated, by measuring the resistance between two emitter contacts for a set of different active emitter lengths. Resistance values $R_{\mathbf{m}}$ are subtracted and plotted against corresponding length differences. Thus, only the first component of Eq. (6) is left. The slope of the resulting $\triangle R_{\mathbf{m}}$ vs $\triangle L_{\mathbf{e}}$ graph gives a number corresponding to the value of $R_{\mathbf{sh}}/w$ [8], where $R_{\mathbf{sh}}$ is the sheet resistance and w - width of the layer. From this slope the sheet resistance can be calculated.

In [9] three methods of performing the differential extraction of $R_{\mathbf{sh}}$, each with an increasing degree of complexity and validity, are described, where the first one is the aforementioned method. The second method takes the radial spreading of the current into account, which is important for large $\triangle L_{\mathbf{e}}$ values. Hence,

$$R_{\mathbf{mj}} - R_{\mathbf{mi}} = R_{\mathbf{sh}} \cdot \alpha_{\mathbf{ij}}^{\mathbf{edge}} \tag{7}$$

and

$$\alpha_{\mathbf{ij}}^{\mathbf{edge}} = \frac{1}{2\pi}\mathbf{ln}[\frac{r+0.5\cdot L_{\mathbf{ij}}}{r-0.5\cdot L_{\mathbf{ij}}}], \tag{8}$$

where indexes $i = 1,...,n$ and $j = 1,...,n$ refer to each specific test structure (with $j > i$) and $L_{\mathbf{ij}} = L_{\mathbf{j}} - L_{\mathbf{i}} = \triangle L_{\mathbf{e}}$.

The third method is applied when the length of subtracted regions become so large, that the radial spreading through these regions cannot be neglected. An accurate differential relationship can be established by subtracting the region of $L_{\mathbf{i}}$ at the center of $L_{\mathbf{j}}$ rather than at the edges [9]. Thus,

$$R_{\mathbf{mj}} - R_{\mathbf{mi}} = R_{\mathbf{sh}} \cdot \alpha_{\mathbf{ij}}^{\mathbf{edge}} \tag{9}$$

and

$$\alpha_{\mathbf{ij}}^{\mathbf{edge}} = \frac{1}{2\pi}\mathbf{ln}[\frac{(r-0.5\cdot L_{i})(r+0.5\cdot L_{\mathbf{j}})}{(r+0.5\cdot L_{\mathbf{i}})(r-0.5\cdot L_{\mathbf{j}})}]. \tag{10}$$

To show the validity of the calculated value, the sheet resistance can also be derived with [8]:

$$R_{\mathbf{sh}} = \frac{\rho}{d} = \frac{1}{q\int_0^\infty \mu_p(x)\cdot N(x)_{\mathbf{A}}dr} \approx \frac{1}{\mu_p q N_{\mathbf{A}} d} \tag{11}$$

where N is the doping concentration of the active emitter layer. The value of μ_p is directly taken from the simulations using the cutline function.

C. *Ideality factor*

The ideality factor of a diode is a measure of how closely the diode follows the ideal diode equation. The ideal diode equation assumes that all the recombination occurs via band to band or recombination via traps in the bulk areas (i.e. quasi-neutral areas) from the device. Using that assumption, the derivation produces the ideal diode equation with ideality factor n of 1 [10]:

$$I = I_0 \cdot (e^{\frac{V}{n\cdot u_T}} - 1) \tag{12}$$

where I is the current through the diode, V - voltage across the diode, I_0 - dark saturation current and n - ideality factor. For relatively high forward voltage values the -1 term can be neglected.

However, recombination does occur in other ways and in other areas of the device, e.g. recombination inside the depletion region (SRH recombination [8]). This type of recombination produces an ideality factor that deviates from the ideal case. In order to calculate the ideality factor, log of both sides of Eq. (12) can be taken:

$$\mathbf{ln}(I) = \mathbf{ln}(I_0) + \frac{1}{u_T\mathbf{ln}(10)} \cdot V \tag{13}$$

When plotting the natural log of the current against the voltage, the slope gives $u_T\mathbf{ln}(10)/n$ and the intercept gives $\mathbf{ln}(I_0)$. Thus, the ideality factor can be found from the slope (for 0.4 V) (see Figure 4):

$$n = \frac{(\frac{\partial \mathbf{log} I}{\partial V})^{-1}}{u_T\mathbf{ln}(10)} = \frac{(1.66/0.1)^{-1}}{0.0596} \approx 1 \tag{14}$$

Ideality factors $n \leq 1.1$ are satisfactory for profiling [11]. When n approaches 2 recombination current dominates.

IV. Results

A. Surface recombination

Figure 4 illustrates the Gummel plot taken from simulations of the structure (for $L_\mathbf{e} = 44\mu$m). Base current values for each active emitter length at 0.4V were derived, and subtracted current values were plotted against the length differences (see Figure 5).

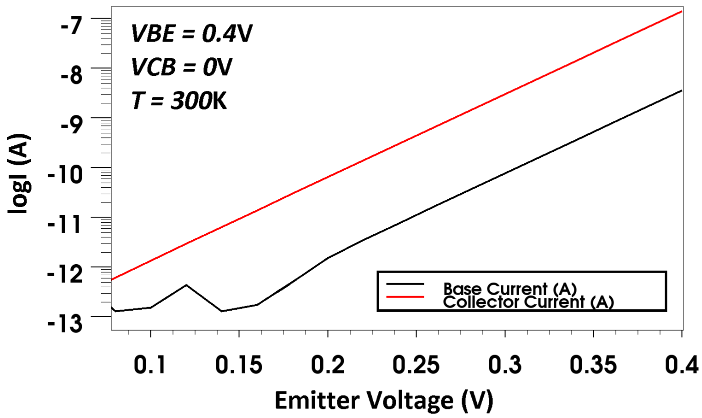

Fig. 4: Gummel plot for $L_e = 44\mu$m obtained from simulations

Using Eq. (2) for a cylindrical structure $J_\mathbf{n}$ can be calculated:

$$J_\mathbf{n} = \frac{\triangle I_\mathbf{b}}{2\pi r \cdot \triangle L_\mathbf{e}} = \frac{7.97 \cdot 10^{-10}}{2\pi \cdot 68.5 \cdot 10^{-6} \cdot 10 \cdot 10^{-6}} \approx 1.8 \cdot 10^{-5} \mathbf{A/cm^2} \quad (15)$$

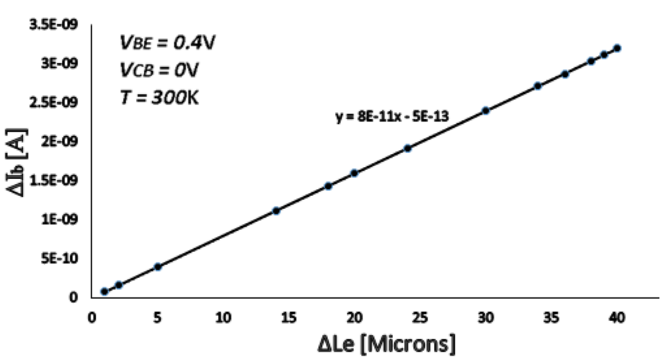

Fig. 5: $\triangle I_b$ plotted against subtracted active emitter layer length ($\triangle L_e$) extracted from cylindrical structures

Figure 6 illustrates the electron concentration and $J_\mathbf{n}$ of the active emitter layer. The value of $J_\mathbf{n}$ was found to be around $1.6 \cdot 10^{-5} \mathbf{A/cm^2}$, which is very close to the value calculated in Eq. (15).

From Figure 6 it can be seen that the minority carriers show a near linear decrease towards the electrode. In case of a short distance between the electrode and the edge of the depletion layer exponential decay, which is inherent to the recombination process, can be approximated by a linear decay. However, due to some bulk recombination inside the layer simulated line is not perfectly linear.

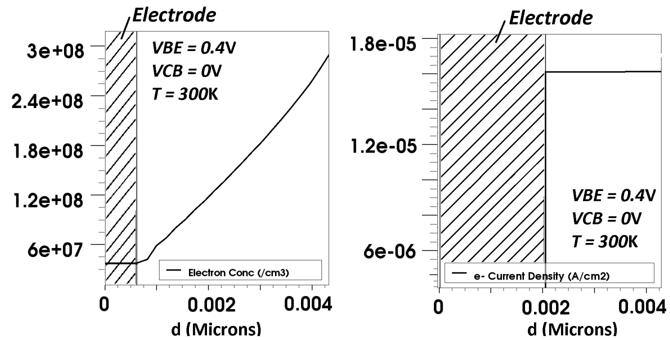

Fig. 6: Electron concentration and $J_\mathbf{n}$ simulated using cutline function

By substituting values of electron concentrations into Eq. (3), the value of electron current density was derived:

$$J_\mathbf{n} \approx q D_n \cdot \frac{n_2}{d} = = 0.4975 \cdot 1.602 \cdot 10^{-19} \cdot \frac{2.8438 \cdot 10^8}{4.56 \cdot 10^{-6} - 3.36 \cdot 10^{-6}} \approx 1.88 \cdot 10^{-5} \mathbf{A/cm^2} \quad (16)$$

All three methods gave similar results, meaning that the test structures are suitable for active emitter region analysis.

As a next step, in order to see the relation with the lifetime, the surface recombination in the active emitter area was varied. The electron current density was simulated for the cylindrical structure, and the results showed that $J_\mathbf{n}$ is decreasing horizontally from emitter 1 to emitter 2 (see Figure 9). Therefore, with increasing active emitter region length, the horizontal variation of $J_\mathbf{n}$ also increased (see Table II). Hence, there is a non-uniform current flow for large cylindrical structures. Figure 7 shows the electron current density contour of the simulated structure for two different $L_\mathbf{e}$ values. This figure also indicates that for large $L_\mathbf{e}$ the current flowing from base 1 to emitter 1 is higher than the current flowing from base 2 to emitter 2. The reason of that is the radial spreading of the current in cylindrical structures, even at low injection.

To calculate the value of $J_\mathbf{n}$, base current subtraction method for $S_\mathbf{eff} = 10^4 \mathbf{cm/s}$ was applied (see Figure 8):

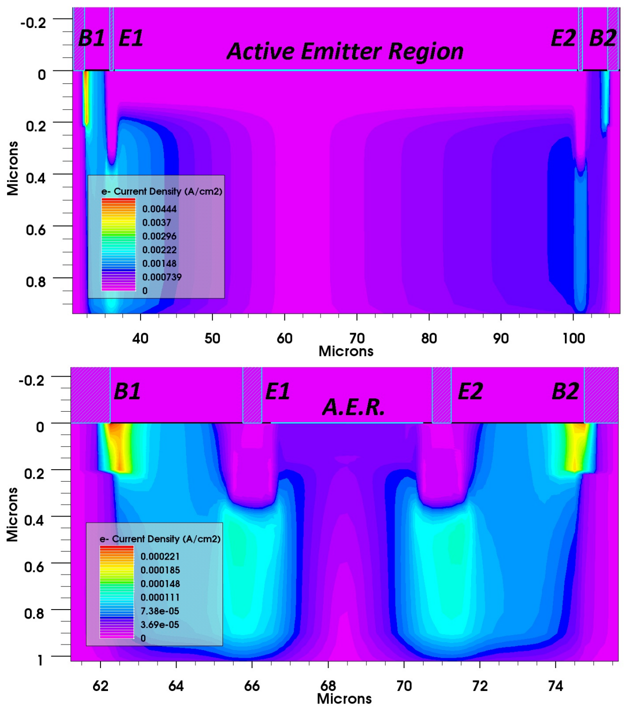

Fig. 7: Electron current density contour plot in a cylindrical structure for $L_{\mathbf{e}} = 64\mu$m and $L_{\mathbf{e}} = 4\mu$m

TABLE II: Difference in electron current density for different active emitter region lengths (see Figure 9)

$L_{\mathbf{e}}[\mu$m]	J_1[A/cm2]	J_2[A/cm2]
4	$3.016 \cdot 10^{-5}$	$2.89 \cdot 10^{-5}$
10	$3.12 \cdot 10^{-5}$	$2.7826 \cdot 10^{-5}$
20	$3.3556 \cdot 10^{-5}$	$2.6259 \cdot 10^{-5}$
24	$3.4537 \cdot 10^{-5}$	$2.5707 \cdot 10^{-5}$
34	$3.7249 \cdot 10^{-5}$	$2.4366 \cdot 10^{-5}$
44	$4.0446 \cdot 10^{-5}$	$2.32 \cdot 10^{-5}$
64	$4.87 \cdot 10^{-5}$	$2.11 \cdot 10^{-5}$

$$J_{\mathbf{n}} = \frac{\triangle I_{\mathbf{b}}}{2\pi r \cdot \triangle L_{\mathbf{e}}} = \frac{1.25 \cdot 10^{-10}}{2\pi \cdot 68.5 \cdot 10^{-6} \cdot 10^{-6}} \approx 2.9 \cdot 10^{-5} \mathbf{A/cm^2} \quad (17)$$

For small $L_{\mathbf{e}}$ the horizontal component of electron current density can be assumed to be constant, and the result of Eq. (17) matches with the simulation results (for $S_{\mathbf{eff}} = 10^4 \mathbf{cm/s}$). However, for large $L_{\mathbf{e}}$ the variation in current density becomes more significant (see Table II) and derived $J_{\mathbf{n}}$ cannot be compared to simulation results. For confirmation, the structure was changed to 2D, and here a constant $J_{\mathbf{n}}$ component was observed irrespective of the $L_{\mathbf{e}}$ value. This implies that the current flow is strongly affected by the curvature of the cylindrical structures, unlike in 2D structures.

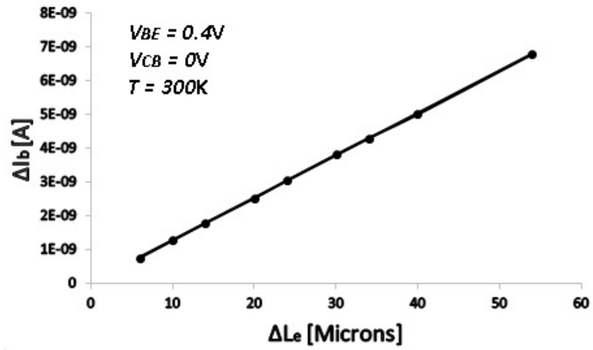

Fig. 8: Electron current density simulated with horizontal cutline through active emitter region

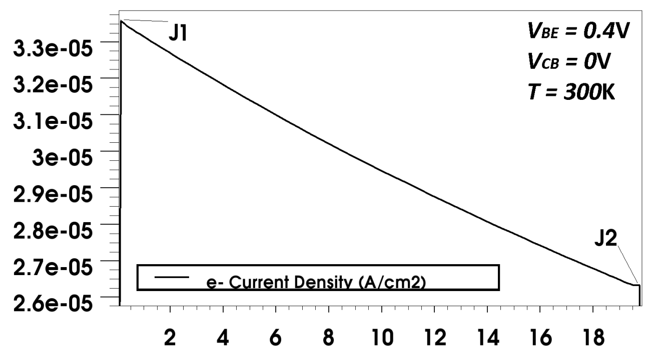

Fig. 9: Electron current density simulated with horizontal cutline through active emitter region for $L_{\mathbf{e}} = 20\mu$m

For an additional check for the 2D structure, $J_{\mathbf{n}}$ for different surface recombination values was simulated (see Table III). Figure 10 illustrates the Gummel plot of the base currents plotted for different surface recombination velocity values [12], showing that the increase in $S_{\mathbf{eff}}$ provokes the increase of the base current. This behaviour is in agreement with Eq. (5).

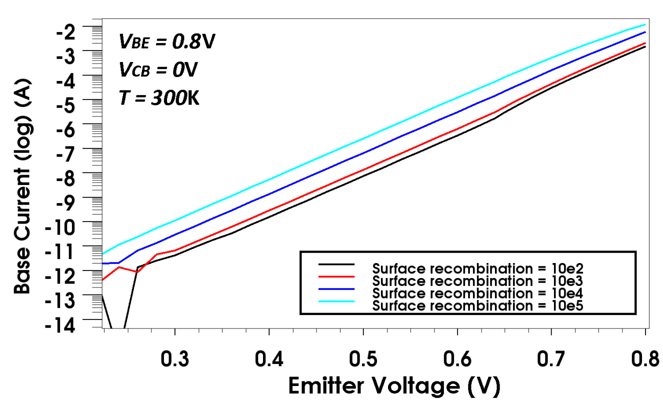

Fig. 10: Gummel plot of the base currents for different surface recombination velocities

The electron current density was also calculated by substituting the values of surface recombination and electron concentration into Eq. (5):

$$J_{\mathbf{n}} = q \cdot S_{\mathbf{eff}}(n_1 - n_0) = 1.602 \cdot 10^{-19} \cdot 10^5 \cdot (8.6517 \cdot 10^8 - \frac{10^{22}}{7.12 \cdot 10^{19}}) \approx 1.4 \cdot 10^{-5} \mathbf{A/cm^2} \quad (18)$$

The calculated value (for $S_{\mathbf{eff}} = 10^5$cm/s) matched with the simulated one (see Table III).

As in case of the cylindrical structure, base current values for each active emitter length at 0.4V for $S_{\mathbf{eff}} = 10^5$cm/s were derived, and subtracted current values were plotted against the length differences (see Figure 11). Since the simulated structure is here 2D, following formula was used to calculate electron current density:

$$J_{\mathbf{n}} = \frac{\triangle I_{\mathbf{b}}}{\triangle L_{\mathbf{e}}} \approx 1.43 \cdot 10^{-5} \mathbf{A/cm^2} \quad (19)$$

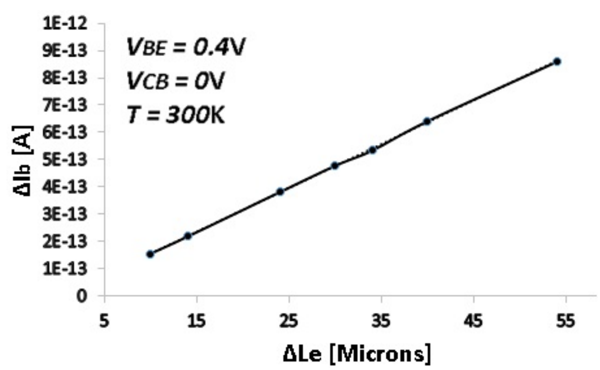

Fig. 11: $\triangle I_b$ plotted against subtracted active emitter layer length extarcted from 2D structures (for $S_{\mathbf{eff}} = 10^5$cm/s)

So, Eqs. (18) and (19), as well as simulation results (see Table III), gave similar results, meaning that the effect of added surface recombination is correct. This experiment has been done for different surface recombination values. However, for much lower values (e.g. $S_{\mathbf{eff}} = 10^2$cm/s) derived electron current density did not match with the results from Table III. The reason for that could be that the electron current flowing from base to emitter is much higher than the current flowing to the active emitter region, and for very low surface recombination values $J_{\mathbf{n}}$ becomes negligibly low. Since then surface recombination is less important, this is no issue.

These experiments imply that indeed lifetime in solar cells can be extracted using this test structure.

TABLE III: Relation between simulated electron current density and surface recombination

$J_{\mathbf{n}}$ [$\mathbf{A/cm^2}$]	$S_{\mathbf{eff}}$ [$\mathbf{cm/s}$]
$1.5 \cdot 10^{-8}$	10^2
$1.49 \cdot 10^{-7}$	10^3
$1.48 \cdot 10^{-6}$	10^4
$1.39 \cdot 10^{-5}$	10^5

TABLE IV: Sheet resistance derived with three different methods reported in [9]

$L_{\mathbf{ij}}$ [μm]	$R_{\mathbf{sh}}$ (M1) [Ω]	$R_{\mathbf{sh}}$ (M2) [Ω]	$R_{\mathbf{sh}}$ (M3) [Ω]
1	173.5184	173.5147	173.326
2	173.4375	173.4315	173.2031
4	173.8955	173.8521	173.2928
6	173.6621	173.6247	173.2522
16	183.6515	182.7897	173.367
20	182.5151	181.2219	173.3685
24	178.4732	176.6424	173.3502
56	190.0457	178.9422	173.402
59	189.2097	176.8695	173.377

B. Sheet Resistance

To find the sheet resistance, 0.4V was applied on emitters of the cylindrical structures with different active emitter layer lengths. From the I-V curves resistance values were derived (see Figure 12).

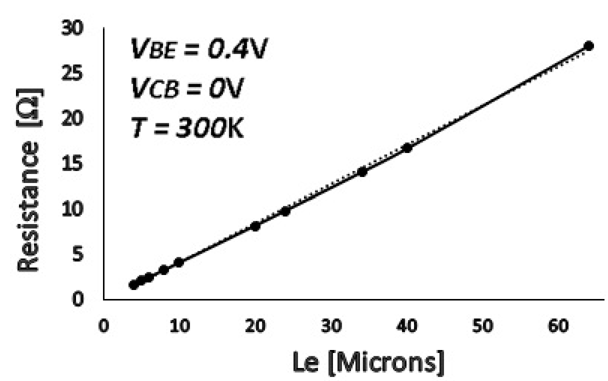

Fig. 12: Simulated resistance values plotted against active emitter layer length for cylindrical structure

As explained in section III, three methods of deriving sheet resistance were used. Table IV summarizes sheet resistance values derived for different subtracted active emitter region length values. Ideally, different subtracted length values with the corresponding resistance values from Figure 12 should give the same sheet resistance. From Table IV, it is clearly seen that the sheet resistance value obtained from the first and second methods fluctuate, whereas the third method gives a constant number, meaning that it is more accurate.

From Eq. (9) and (10):

$$R_{\mathbf{sh}} = \frac{R_{\mathbf{mj}} - R_{\mathbf{mi}}}{\alpha_{\mathbf{ij}}^{\mathbf{edge}}} = \frac{R_{\mathbf{mj}} - R_{\mathbf{mi}}}{\frac{1}{2\pi} ln[\frac{(r-0.5\cdot L_{\mathbf{i}})(r+0.5\cdot L_{\mathbf{j}})}{(r+0.5\cdot L_{\mathbf{i}})(r-0.5\cdot L_{\mathbf{j}})}]} \approx 173\Omega/\square \quad (20)$$

To check the validity of the sheet resistance value calculated using the third method, Eq. (11) was used:

$$R_{\mathbf{sh}} = \frac{\rho}{d} = \frac{1}{\mu_n q N d} = \frac{1}{30 \cdot 1.602 \cdot 10^{-19} \cdot 10^{21} \cdot 1.2 \cdot 10^{-6}} \approx 173\Omega/\square, \quad (21)$$

where the value of the electron mobility $\mu_{\mathbf{n}}$ was taken from simulations using the cutline function.

As Eqs. (20) and (21) gave the same result, it can be concluded that the surface channel sheet resistance of the structure with an oxide layer on top of the active emitter layer was derived correctly.

Unfortunately, actual sheet resistance measurements of the structure with an oxide layer on top were not available. Therefore, the values calculated from simulations could not be compared to the measured data.

V. Conclusion

In this paper, dedicated phototransistor test structures, all imitating a solar cell, were simulated. By varying the length of the active emitter layer, the actual value of the electron current density was found. Several methods were used to show the validity of this value. In turn, from the electron current density the surface recombination or lifetime can be extracted, showing that these structures are suitable for analysing the efficiency of solar cells. Difference between the cylindrical and 2D structures was observed, as the horizontal component of the electron current density at the active emitter region of the cylindrical structure showed a non-uniform behaviour due to radial spreading. Therefore, further comparison of different methods of extraction of the electron current density value for cylindrical structure with large $L_{\mathbf{e}}$ was not possible. For this 2D structures are advised.

In addition, the differential measurement technique using the test structure has been demonstrated to be a technique of accurately determining the surface channel sheet resistance. This allows a direct comparison with the sheet resistance measured in the lab.

For future research it is suggested to use more realistic profiles of the structure to be able to compare simulation results with the actual measurement results.

VI. Appendix

First, an artificial contact is considered on top of the active emitter region. In this way possible bulk and/or interfacial recombination effects are incorporated in a single parameter called (effective) surface recombination velocity $S_{\mathbf{eff}}$ [13], [14].

From the change in carrier density due to the difference between the incoming and outgoing flux of carriers the following continuity equation is derived [15]:

$$\frac{1}{q} \cdot \frac{\partial J_{\mathbf{n}}}{\partial x} = \frac{n(x)}{\tau} \quad (22)$$

where

$$n = n_1 \cdot e^{\frac{x-w}{L}} \quad (23)$$

with w - artificial contact thickness and L - diffusion length. Hence,

$$J_{\mathbf{n}} = q \cdot \int_0^w \frac{n_1}{\tau} \cdot e^{\frac{x-w}{L}} dx \quad (24)$$

Assuming $w \gg L$:

$$J_{\mathbf{n}} = \frac{q n_1 L}{\tau} = q\sqrt{\frac{D_n}{\tau}} \cdot n_1 \equiv q \cdot S_{\mathbf{eff}}(n_1 - n_0) \quad (25)$$

Therefore,

$$S_{\mathbf{eff}} \equiv \sqrt{\frac{D_n}{\tau}} \quad (26)$$

However, in case of an ultra-thin interfacial layer in which the minority concentration drops to equilibrium value n_0 (e.g. oxide layer), the derivation changes. Assuming $0 \ll L \ll \delta \ll w$, where δ is the thickness of the interface (e.g. silicon-dioxide interface):

$$J_{\mathbf{n}} \approx \lim_{\delta \to 0} q \frac{\delta}{\tau} (\frac{n_1 - n_0}{2} + n_0) \approx \lim_{\delta \to 0} q \frac{\delta}{2\tau} n_1 \quad (27)$$

Thus,

$$S_{\mathbf{eff}} \equiv \lim_{\delta \to 0} \frac{\delta}{2\tau} \quad (28)$$

So, Eqs. (26) and (28) show the relation between effective recombination velocity and carrier lifetime.

REFERENCES

[1] Islam, K., and Nayfeh, A. ”Simulation of a-Si/c-GaAs/c-Si Heterojunction Solar Cells.” Computer Modeling and Simulation (EMS), 2012 Sixth UKSim/AMSS European Symposium : 466-470.

[2] Neugroschel, A. ”Determination of lifetimes and recombination currents in pn junction solar cells, diodes, and transistors.” Electron Devices, IEEE Transactions on 28.1 (1981): 108-115.

[3] Gonzalez, F. N, and Neugroschel, A. ”Measurement of diffusion length, lifetime, and surface recombination velocity in thin semiconductor layers.” Electron Devices, IEEE Transactions on 31.4 (1984): 413-416.

[4] Lederhandler, SRj, and Giacoletto, LJ. ”Measurement of minority carrier lifetime and surface effects in junction devices.” Proceedings of the IRE 43.4 (1955): 477-483.

[5] Macdonald, Daniel, Ronald A Sinton, and Andrs Cuevas. ”On the use of a bias-light correction for trapping effects in photoconductance-based lifetime measurements of silicon.” Journal of Applied Physics 89.5 (2001): 2772-2778.

[6] Fahrenbruch, A. L, and Bube, R. H. Fundamentals of Solar Cells: Photovoltaic Solar Energy Conversion. New York: Academic Press, 1983.

[7] Atlas TCAD process and device simulation software, Silvaco, Inc., Available: http://www.silvaco.com/

[8] Sze, S. M, and Ng. K.K. Physics of semiconductor devices. John wiley and sons, 2007.

[9] Evseev, SB, Nanver, LK and Milosavljevi, S. ”Ring-gate MOSFET test structures for measuring surface-charge-layer sheet resistance on high-resistivity-silicon substrates.” Proc. 19th IEEE Int. Conf. on Microelectronic Test Structures (ICMTS) 6 Mar. 2006: 3-8.

[10] McIntosh K. R. and Honsberg, C. B., The Influence of Edge Recombination on a Solar Cells IV Curve, 16th European Photovoltaic Solar Energy Conference. 2000.

[11] Schroder, D. K. Semiconductor material and device characterization. John Wiley and Sons, 2006.

[12] Touboul A. et al. (1998). Proceedings of the 28th European Solid-State Devices. Bordeaux, France

[13] De Graaff, HC, Slotboom, JW. and Schmitz, A. ”The emitter efficiency of bipolar transistors: Theory and experiments.” Solid-State Electronics 20.6 (1977): 515-521.

[14] Post, I. R.C, Ashburn, P. and Wolstenholme, G.R. ”Polysilicon emitters for bipolar transistors: a review and re-evaluation of theory and experiment.” Electron Devices, IEEE Transactions on 39.7 (1992): 1717-1731.

[15] Hueting R.J.E et al., Semiconductor Devices Explained More., University of Twente, Enschede, The Netherlands, 2013.